Aeolian Research 12 (2014) 143–156

Contents lists available at ScienceDirect

Aeolian Research

journal homepage: www.elsevier.com/locate/aeolia

Wind regime and sand transport in the corridor between the Badain Jaran and Tengger deserts, central Alxa Plateau, China

YanYan Yang [a,c], ZhiQiang Qu [a,c], PeiJun Shi [a,b,c], LianYou Liu [a,b,c,*], GuoMing Zhang [a,c], Yan Tang [d], Xia Hu [a,c], YanLi Lv [b,c], YiYing Xiong [a,c], JingPu Wang [a,c], LingLing Shen [a,c], LiLi Lv [b], Shao Sun [b]

[a] Key Laboratory of Environmental Change and Natural Disaster, Ministry of Education, Beijing Normal University, Beijing 100875, China
[b] State Key Laboratory of Earth Surface Processes and Resource Ecology, Beijing Normal University, Beijing 100875, China
[c] MOE, Engineering Research Center of Desertification and Blown-sand Control, Beijing Normal University, Beijing 100875, China
[d] College of Resources, Environment and Planning, Dezhou University, Dezhou, 253023, China

ARTICLE INFO

Article history:
Received 14 May 2013
Revised 14 December 2013
Accepted 24 December 2013
Available online 11 February 2014

Keywords:
Deserts in Alxa Plateau of China
Sand-transporting wind
Sand transport flux from Badain Jaran to the Tenger desert
Total amount of sand transport

ABSTRACT

The Alxa Plateau in north China is characterized by frequent sand dust storm activity, desertification, various blown sand hazards and extensive sand dunes. Three of China's major sand deserts, the Badain Jaran (BJ), Tengger and Ulan Buh (UB), are distributed in this region. The BJ desert lies to the northwest and is separated from the other two deserts by mountains Yabrai and Alateng. However, the dominant northwest wind could transport sand from the BJ to the other two deserts through several corridors. Locating the sand source for these deserts is fundamental in understanding the formation and evolution of the aeolian landforms. It has been proposed that the sand in the Tengger desert is from the BJ desert. However, evidence supporting the hypothesis is still limited. To estimate the sand contribution of the BJ to the Tengger desert, we measured wind speeds at a 2 m height above the ground for the period from November 2010 to December 2011. We then calculated the amount of sand transport and observed the speed of dune migration in the junction part of the two deserts. Sand-transporting winds ($\geqslant$6.0 m s^{-1}) occurred mostly in spring and winter, and accounted for 16.4% of the total of the year. The prevailing wind directions were NW, WNW and NNW, and were occupied 61.9% of the total frequency of sand-transporting winds. The frequencies of winds decreased with increasing wind speed, and strong wind frequencies ($\geqslant$17.0 m s^{-1}) were 5.3% of the sand-transporting winds. In comparison to adjacent areas, the drift potential in the corridor was several times higher, indicating an obvious effect of narrowing. During the period of observation, 752 sand-transporting events occurred with durations from 10 to 1940 min (32 h). In the corridor, the sand transport flux was 372 tons m^{-1} yr^{-1}, an order of magnitude larger than previous estimation, and the annual total amount of sand transported through the corridor was over 5 million tons, indicating a substantial sand supply from the BJ to the Tengger desert. Sand transport in spring and winter accounted for 99.8% of annual total. The amount of sand transported by a single sand-transporting event varied greatly, up to five orders of magnitude.

1. Introduction

Aeolian sand transport occurs mostly in the world's drylands. It is an important terrestrial process that leads to sand encroachment, dune migration and the formation of desert landscape. Sand encroachment into oases can cause extensive loss of farmland in arid areas, and dune migration can bury residential buildings, railways, highways and other facilities in many desert areas (Zhu et al., 1980; Lei et al., 2003; Dong, 2004). Aeolian sand transport is a complex process affected by many variables, including surface wind conditions (Lancaster, 1985; Anderson and Haff, 1988; Gillette et al., 2001; Zou et al., 2001; Liu et al., 2005), grain size and sand surface moisture (Jackson and Nordstrom, 1998; Wiggs et al., 2004), surface crusting (Leys and Eldridge, 1991; Rice and McEwan, 2001), topography (Iversen and Rasmussen, 1994; Hesp et al., 2005) and vegetation cover (Buckley, 1987; Kuriyama et al., 2005). Numerous previous studies have been conducted to estimate sand transport through both field measurement and theoretical calculation (Bagnold, 1936, 1937, 1941; Kawamura, 1951; Zingg, 1953; Owen, 1964; Lettau and Lettau, 1978; Sørensen, 2004; Al-Awadhi and Al-Awadhi, 2009; Dong et al., 2011; Sherman and Li, 2012; Sherman et al., 2013).

* Corresponding author at: Key Laboratory of Environmental Change and Natural Disaster, Ministry of Education, Beijing Normal University, Beijing, 100875, China. Tel.: +86 10 58802600.
E-mail address: lyliu@bnu.edu.cn (L. Liu).

http://dx.doi.org/10.1016/j.aeolia.2013.12.006
1875-9637/

The Alxa Plateau is one of the most severe sandy desertification areas in China, and on the plateau, the frequency of sand and dust storms has continuously increased in the last 5 decades (Wang et al., 2001; Yao et al., 2008; Lee and Sohn, 2011). Three of China's major sand deserts, the Badain Jaran (BJ), Tengger and Ulan Buh (UB), are distributed in the region (Fig. 1). Studies in this region have focused on orogenesis (Yang, 1978), environmental changes (Wang, 1990; Zhang et al., 1999, 2002; Yang, 2000), and the formation of mega-dunes and lakes (Yan and Wang, 2001; Chen et al., 2004; Dong et al., 2004, 2009, 2013). It has been proposed that the Tengger desert developed from the sand supply of the BJ desert, although little evidence exists to support this assertion (Guo, 1986). On satellite images, distinct sand corridors connecting the BJ and Tengger deserts could be readily recognized, manifesting long distance southeastward dune sand transport. However, studies investigating sand transport in the region are limited (Yao et al., 2007), and there were few detailed studies that quantify sand movement between the deserts. Therefore, in this study, we analyzed the magnitude and frequency of sand-transporting winds and events based on field data, calculated the sand transport flux, and quantitatively determined the contribution of the BJ to the Tengger desert.

2. Study area

The Alxa Plateau (37°N–43° N, 97°E–107° E) is situated in north China. The eastern edge of the plateau is the Helan Mountains, the Langshan Mountains and the Yellow River. To the north, the plateau lies close to the Mongolian Gobi. The plateau is bounded to the west and southwest by the Mazong Mountains and the Longshou and Beida Mountains, respectively (Fig. 1). The plateau has an elevation of 900–1939 m a.s.l., and is defined bioclimatically as a transition zone from semi-arid and arid grasslands to extremely arid desert (Yao et al., 2008). Precipitation is concentrated in the months of July, August and September, with 100–150, 70–100 and 50 mm of annual mean precipitation in the eastern, central and western regions, respectively (China Meteorological Administration, 1994). The mean day-night and summer-winter temperature differences are approximately 30 and 67 °C. The annual strong wind occurs 50–100 days in the northwest and 15–30 days in the southeast. Accordingly, aeolian activity (Fig. 2d) is particularly active in this region, which is one of the sources of sandstorms in China. The dominant plant species are *Chenopodiaceae, Asteraceae, Zygophyllaceae, Rosaceae* and *Leguminosae* (He et al., 2010).

The three deserts cover a total area of 100,000 km^2, approximately one-third of the area of the plateau. The BJ desert covers an area of 49,000 km^2 and is the second largest desert in China (Zhu et al., 2010). More than 50% of the desert is covered by mega-dunes with a height up to 200–300 m. The highest mega-dune is as high as 437 m, possibly the highest dune on Earth and Mars (Qu et al., 2003; Lancaster, 2006; Zimbelman, 2010). More than 100 lakes of different sizes lie among the mega-dunes and are concentrated in the southeast of the desert (Yang, 2000; Dong et al., 2013) (Fig. 2a). The eastern and southern edges of the desert

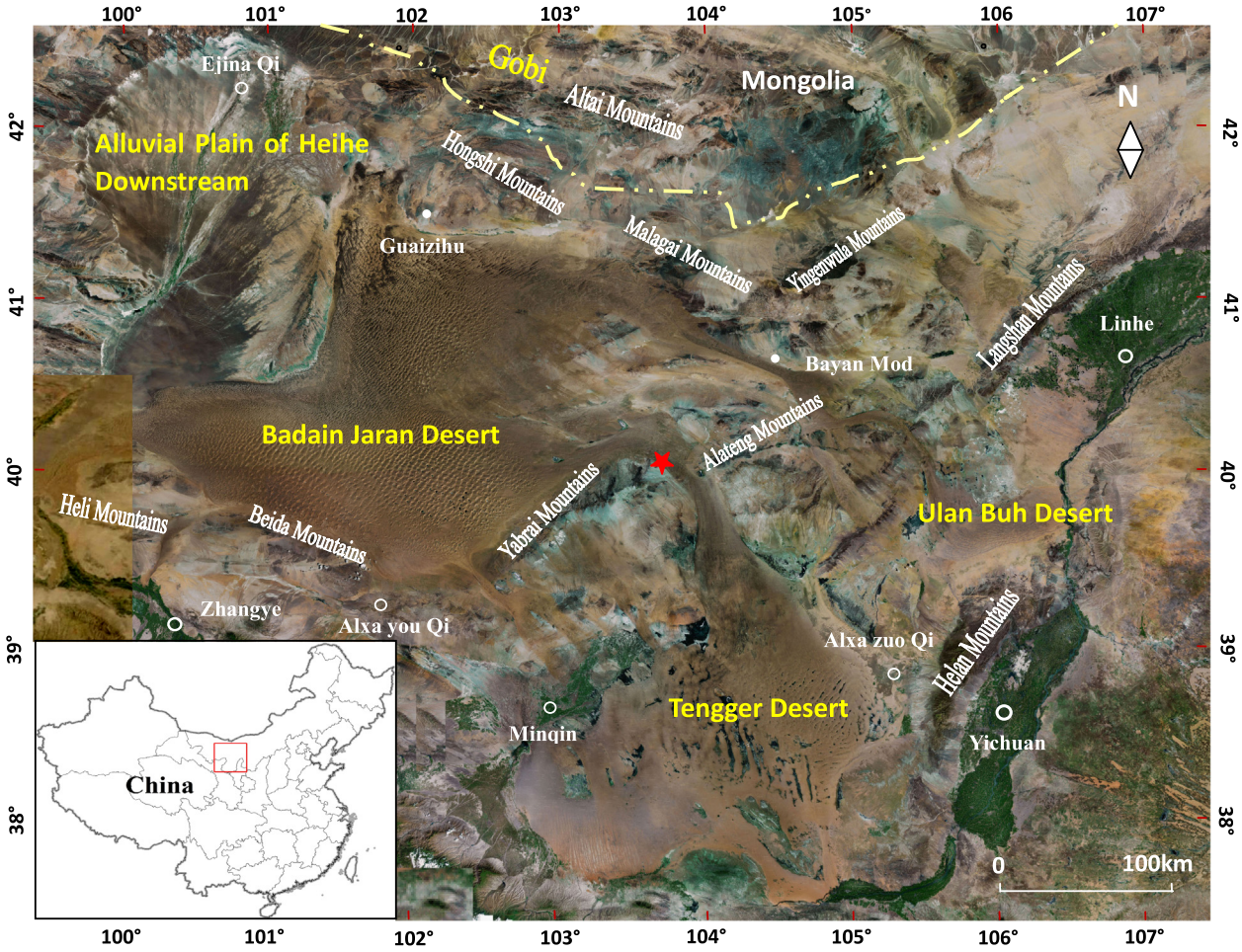

Fig. 1. Location of study area. The red pentagram indicates the location of the observation point. The red rectangle of the bottom left shows the general position of study area in China. The image is TM data, which is from http://www.usgs.gov.

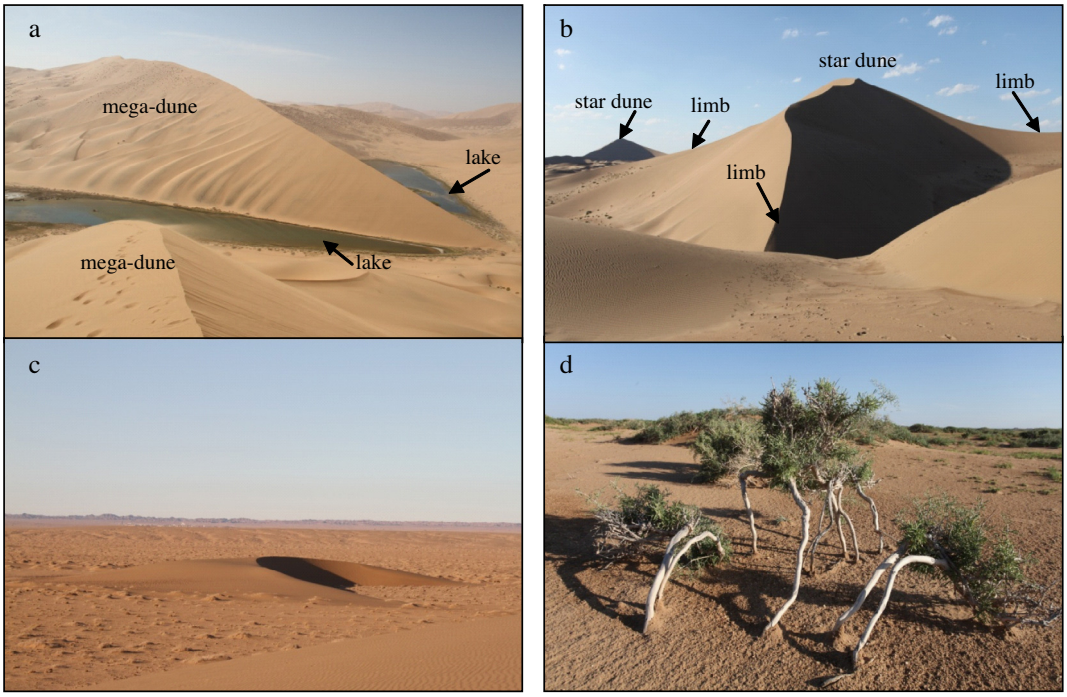

Fig. 2. Typical landforms of Alxa Plateau. (a) Mega dunes and lakes distribute together in BJ desert; (b) star dune in the southwest border of the BJ desert; (c) barchan dune in the corridor of the study (the height is approximately 10 m); (d) severe wind erosion on the ground in the corridor of study. Because wind erosion the roots of *zygophyllum xanthoxylum* are above the ground.

are covered by star dunes, whereas the margin is covered by transverse dunes (Fig. 2b and c). The Tengger desert covers an area of 36,700 km^2, and is the fourth-largest desert in China. More than 420 lakes (mostly saline) of various sizes and extensive latticed dunes are distributed throughout the desert (Zhu et al., 1980). The UB desert covers an area of 10,000 km^2. Shifting, semi-fixed and fixed sand dunes account for 36.9%, 33.3% and 29.8%, respectively, of the region's landscape (Zhu et al., 1980).

Two corridors connect the BJ and Tengger deserts. The first crosses the Yabrai Mountains and spans 100 km in length and 5–45 km in width. The second lies between the Allah Teng (altitude up to 1890 m) and the Yabrai Mountains (altitude up to 1939 m) and has a length and width of 150 and 10–40 km, respectively (Figs. 1 and 3).

Our field observation was conducted in the second corridor, where the local landforms include primarily barchans and barchan chains of various sizes and sand sheets and nebkhas (Fig. 2c and d). The elevation of the corridor decreases from the eastern margin of the BJ desert to the north margin of the Tengger desert, providing favorable topography for sand transport (Fig. 3).

3. Methods and materials

3.1. Wind speed

The wind measurement instrument used in this study was deployed from November 22, 2010 to December 14, 2011 in the area of the junction between the BJ and Tengger deserts (40°03′12.88″ N, 103°51′23.59″ E, 1404 m a.s.l.) (Fig. 1). It consists of a data logger (UGT Data Logger), propeller anemometer, wind vane, temperature sensor, humidity sensor and solar panels (Fig. 4). The climate variables measured included wind speed, relative humidity and air temperature. The anemometer was calibrated in a wind tunnel using standard pitot tubes before measurement in the field. Wind speeds at 2 m above the ground were measured using the anemometer with fixed measurement intervals of 10 min. This measurement height was used because many studies have demonstrated that wind speeds at 2 m are well correlated with sand transport (Wu, 2010; Liu et al., 2005). Data were collected every three months.

Meteorological data from 1973 to 2012 for Bayan Mod, Ejin Qi, Guaizihu and Minqin stations were obtained from the National Climatic Data Center (NCDC) Global Integrated Surface Hourly (ISH) database (NCDC, 2011) (Table 1). The ISH database includes worldwide surface weather observations from 20,000 stations, collected and stored by sources including the Automated Weather Network (AWN), Global Telecommunications System (GTS) and Automated Surface Observing System (ASOS). Quality control analysis of these data demonstrates that errors occur in less than 0.1% of the NCDC data (Deganto, 1997). Wind speeds for all stations were recorded at 4 h intervals; however, in some cases, wind speeds were not recorded in the late evening or early morning. Data bias because of the absence of nocturnal winds was not considered to be an issue in this study because sand transport is believed to take place only at wind speeds $\geqslant$6 m s^{-1} (Bagnold, 1941; Liu et al., 2005). For each station, a total of 1.01–1.16 $\times$ 10^5 wind records were examined, of which 3.8–37.5% exceeded the 6 m s^{-1} threshold which was believed to be required to transport sand (Bagnold, 1941) (Table 1).

3.2. Analysis of sand-transporting events

Wind is a dynamic force in deserts responsible for sand transport when wind speeds exceed a given threshold. The threshold at a height of 2 m above the ground is typically 5–6 m s^{-1} in arid shifting sand environments (Stout, 2004, 2007; Wu, 2010; Barchyn and Hugenholtz, 2012). In this study, a sand-transporting event is defined as a duration in which all wind speeds were continuously greater than or equal to 6 m s^{-1}. A given sand-transporting event is assumed to terminate once the instantaneous wind speed drops below 6 m s^{-1}.

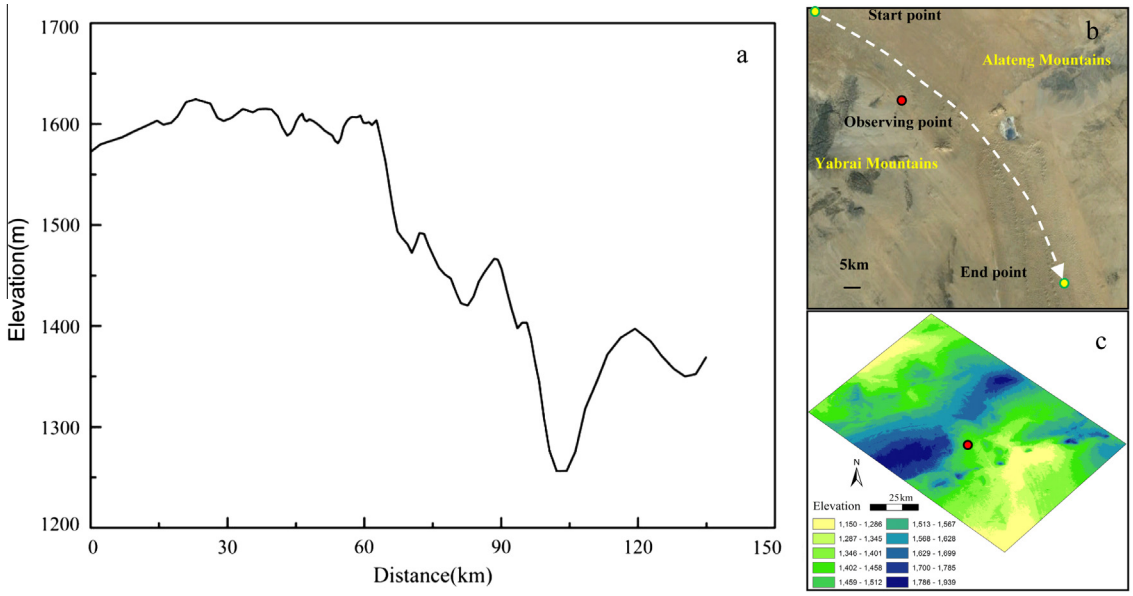

Fig. 3. Topography of the corridor between the BJ and the Tengger deserts and surrounding areas. (a) Is the elevations variation from start point to the end point of the corridor, along the central axis showing arrow dotted line (b), and the location of the measurement filed; (b) is the central axis of the corridor; (c) is DEM of the corridor and surrounding areas. This illustrates that the corridor is located between two mountains. The red dot marks observing filed the same with (b). The data of elevation data are from http://datamirror.csdb.cn/index.jsp and the resolution is 30 m. The image of (b) is from GoogleEarth. (For interpretation of the references to color in this figure legend, the reader is referred to the web version of this article.)

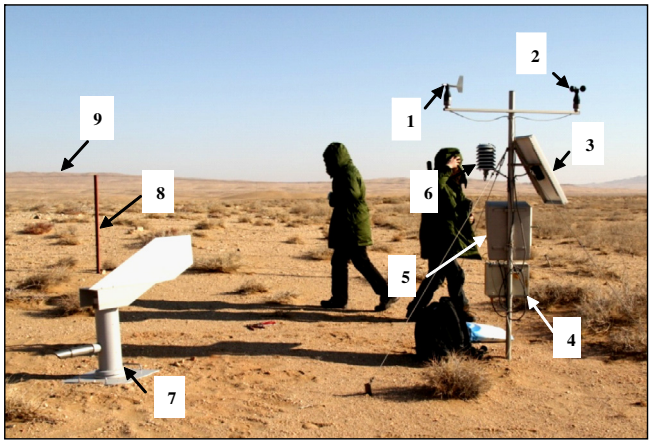

Fig. 4. Instruments used to measure meteorological data. (1) Wind vane. (2) Propeller anemometer. (3) Solar panels. (4) Battery. (5) Datalogger. (6) Temperature and humidity sensor. (7) Sediment collector. (8) Fence. (9) Shifting dune.

3.3. Calculation methods

3.3.1. Sand transport calculation

The sand transport rate was calculated using the equation of Lettau and Lettau (1978):

$$q = C_b\sqrt{d/D}\frac{\rho}{g}(U_* - U_{*t})(U_*)^2, \quad (1)$$

where q is the amount of sand transported per meter per second (kg m^{-1} s^{-1}); C_b is a constant (4.3; Sherman et al., 1998); d is the grain size for the study site (0.27 mm; Table 2); D is a reference grain size (0.25 mm); ρ is the air density (held constant at 1.22 kg m^{-3}); g is the acceleration due to gravity (9.81 m s^{-2}), and U_* and U_{*t} are the surface friction velocity and threshold friction velocity, respectively. The surface friction velocity was determined by rearranging the law of the wall as follows (Sherman et al., 1998):

$$U_* = \frac{\kappa U_z}{\ln(z/z_0)}, \quad (2)$$

where κ is von Karman's constant (0.41). U_z is the wind speed at elevation z (2 m), and z_0 is the aerodynamic roughness length,

Table 1
Meteorological data stations information.

Station(ID)	Lat./lon.	Elevation	Period of record used	Total records	Records ⩾ 6 m s^{-1} (% of total)	DP
BaYan Mod(524950)	40.75/104.50	1329 m	1973–2012	113783	24,925(21.9%)	220.5
Ejin Qi(522670)	41.95/101.07	941 m	1973–2012	116119	16,871(14.5%)	176.9
Guaizi Hu(52378)	41.37/102.37	960 m	1973–2012	100527	37,677(37.5%)	245.7
Minqin(526810)	38.63/103.08	1367 m	1973–2012	116194	10,667(9.2%)	194.4

Table 2
The grain size of the study area.

Particle-size grading (mm)	<0.002	0.002–0.0625	0.0625–0.125	0.125–0.25	0.25–0.5	0.50–1.00	>1.00
Volume percent (%)	1.40	5.76	3.42	35.19	49.66	4.59	0.00

which is assumed to be 1/30th of the mean grain size. U_{*t} is the value when U_z is equal to 6 m s^{-1} at a 2 m height. Assuming a total transport time of 10 min, the amount of sand transported during each 10 min measurement interval (q_t) was calculated as follows:

$$q_t = 600q, \tag{3}$$

where q is calculated from Eq. (1).

Calculation of the resultant sand transport flux, the annual amount of sand transported in unit width requires consideration of the speed, duration of sand transporting wind in all 16 directions. To obtain q_c (the calculated resultant sand transport flux), we assumed that all amount sand transport (q_t) in different directions in 10 min occurred in the horizontal plane and orthogonally decomposed q_t into two different directions within the same coordinate system, such that the x-axis and y-axis represented east–west and north–south transport, respectively. q_t has two components, q_x and q_y:

$$q_x = q_t \sin\beta, \tag{4}$$

$$q_y = q_t \cos\beta, \tag{5}$$

where β is the angle between the wind direction and north (0–360°).

The calculated resultant sand transport flux (q_c) was obtained by:

$$q_c = \sqrt{\left(\sum q_x\right)^2 + \left(\sum q_y\right)^2}, \tag{6}$$

The resultant drift direction (RDD) is expressed as the direction of the net trend of sand drift:

$$\mathrm{RDD} = \arctan\left(\sum q_x / \sum q_y\right), \tag{7}$$

In the final, q_c was rectified by the formula proposed by Al-Awadhi and Al-Awadhi (2009):

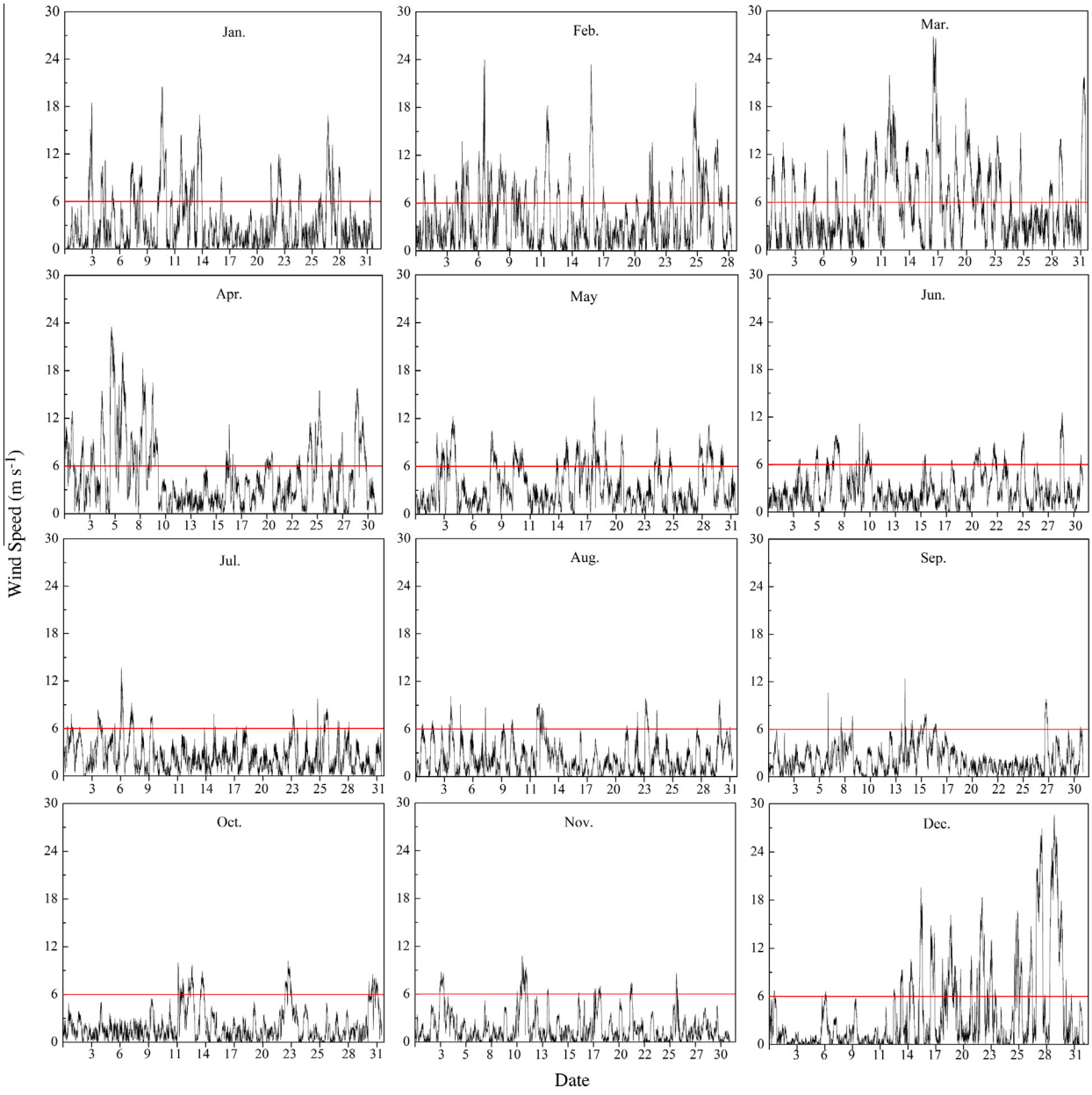

Fig. 5. Distribution of wind speed in different months. The red line is the threshold of wind speed (6 m s^{-1}). The x-axis is the date of each month. (For interpretation of the references to color in this figure legend, the reader is referred to the web version of this article.)

$$q_{cr} = C_L q_c, \quad (8)$$

where q_{cr} is the rectified resultant sand transport flux, expressing total annual sand transport in unit width in the study area, and C_L is a coefficient for rectification (0.558).

3.3.2. Drift potential calculation

Wind speeds at a height of 2 m were converted to wind speeds at 10 m using the equation of Liu et al. (2005):

$$V_{10} = 1.16 \times V_2 + 0.81, \quad (9)$$

where V_2 and V_{10} represent wind speeds at heights of 2.0 m (in the observation field) and 10 m, respectively.

The drift potential (DP) was calculated according to the equation of Fryberger and Dean (1979):

$$\mathrm{DP} = V_{10}^2 \times (V_{10} - V_t) \times t, \quad (10)$$

where V_{10} is the recorded wind speed ($\geqslant 6\ \mathrm{m\ s^{-1}}$) at a height of 10 m; V_t is the threshold wind speed ($6\ \mathrm{m\ s^{-1}}$ in this case). t is the time increment relative to the total time for all measurements expressed as a percentage. The total DP is represented by values obtained according to Eq. (10), summed for all wind directions over a given amount of time (e.g., yearly or monthly). Fryberger and Dean (1979) defined low, intermediate and high DP as being <200, 200 < DP < 400 and $\geqslant$400, respectively.

3.4. Dune migration and height measurement

A Landsat Enhanced Thematic Mapper Plus image in August 1999 (ETM+ image, band 8, 15 m per pixel) and an Advanced Land Observing Satellite image in September 2009 (ALOS image, 2.5 m per pixel) were used to observe dune migration in the study area. The quality of the images was good enough for our purpose, with no cloud cover obscuring the areas of interest. We used the level 1T and level 1B2 images, conducting orthographic projection of these images in the ENVI software using several topographic maps (1:50,000) produced by surveys. Then, the two images, which have different resolutions of 15 and 2.5 m, respectively, were resampled to a common ground resolution of 10 m using ArcGIS 10. Finally, mapping of dune outlines, measurement of dune perimeters and areas and calculation of dune migration speeds were conducted according to the methods described by Yao et al. (2007).

In August 2011, we used a differential global positioning system (G9-RKT; vertical accuracy of 15 mm + 1 ppm) to measure dune height. Dune height (H) can also be derived according to the relationship $H = L \sin\alpha$, where L and α are the length and angle of repose of the slip face, respectively. Based on measurements of sample dunes in the study area, sin α was approximately 0.5. Therefore, we calculated dune heights using the length of the slip face of dunes in the ALOS image of 2009 (2.5 m per pixel).

4. Results and discussion

4.1. Sand-transporting winds

Our results demonstrated that wind speeds fluctuated widely during the study period. The maximum wind speed ($28.6\ \mathrm{m\ s^{-1}}$) occurred in December. Moreover, maximum wind speeds were above $20\ \mathrm{m\ s^{-1}}$ in spring and winter (except May) and below $15\ \mathrm{m\ s^{-1}}$ in summer and autumn (Fig. 5). Sand-transporting winds accounted for 16.4% of the entire year duration. The frequencies of sand-transporting winds decreased with increasing wind speed. The frequency of normal winds (<$17\ \mathrm{m\ s^{-1}}$) accounted for 94.7% of sand-transporting winds and 15.5% of the entire year, whereas strong winds were observed during 5.3% of sand-transporting winds and 0.9% of the year (Fig. 6). The frequency of strong winds was higher than that reported in observations by Liu et al. (2005), which were in the Yijinhole and Dalate stations, only 0.6% and 0.2% of a year. Therefore, sandstorms were frequent and aeolian sand activity was stronger in this area.

The sand-transporting winds occurred primarily in spring and winter, particularly in March, when the frequency of sand-transporting winds reached its maximum, accounting for 36.8% of this month duration. Winds with a speed of $9\ \mathrm{m\ s^{-1}}$ were more frequent than those at other speeds in this month, occurring 15.1% of the sand-transporting wind duration. While strong winds were more frequent than other winds in December and occurred 20.8% of sand-transporting wind duration. Overall, the sand-transporting winds were the least frequent in September, and occurred during only 3.6% of the month duration (Fig. 7).

Sand-transporting winds were observed in three prevailing directions, NW, WNW and NNW, making up 61.9% of the total frequency of sand-transporting winds. The respective frequencies of the prevailing winds in NW, WNW and NNW, were 10.4%, 10.1% and 5.1% in spring; 4.5%, 2.2% and 1.9% in summer; 2.9%, 2.4% and 0.5% in autumn; and 9.9%, 8.8% and 3.0% in winter. Thus, the highest frequencies of sand-transporting winds were observed in spring, although the highest frequencies of winds in the three prevailing directions occurred during different months. March, April and May were the months with the highest frequencies of 2.23%, 3.51% and 3.79% in the NNW, WNW and NW directions, respectively, whereas the lowest frequencies of prevailing directions were observed in August, which were 0.3%, 0.3% and 0.06%, respectively. The wind frequencies along the NE direction were 2.6%, 0.8%, 1.5% and 2.1% in spring, summer, autumn, and winter, respectively, which were only lower than those in the three prevailing wind directions. The NE direction was the prevailing direction in September (Fig. 8). This occurred likely because the research area is located at the southeastern outer edge of a zone of high atmospheric pressure from Mongolia that generates in September (early autumn), when the influence of the pressure gradient force, the Coriolis force and friction results in the clockwise flow of pressure isobars in the Northern Hemisphere.

Except September, the prevailing directions of sand-transporting winds were NW, WNW, NNW in the most of the year, the corridor was almost under unidirectional northwest winds. Moreover, sand availability is limited in the study area because it is located at the edge of the BJ desert. Therefore, massive barchans and barchains are distributed throughout the corridor, providing empirical evidence for the theory of barchan formation (Wasson and Hyde,

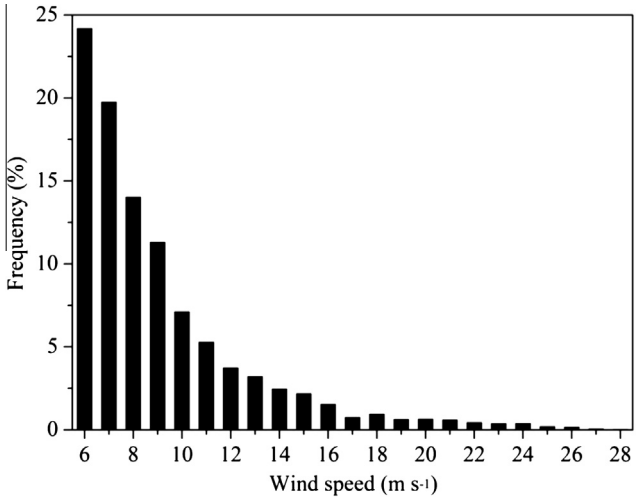

Fig. 6. Frequency (%) of sand-transporting wind at different wind speed levels throughout the year.

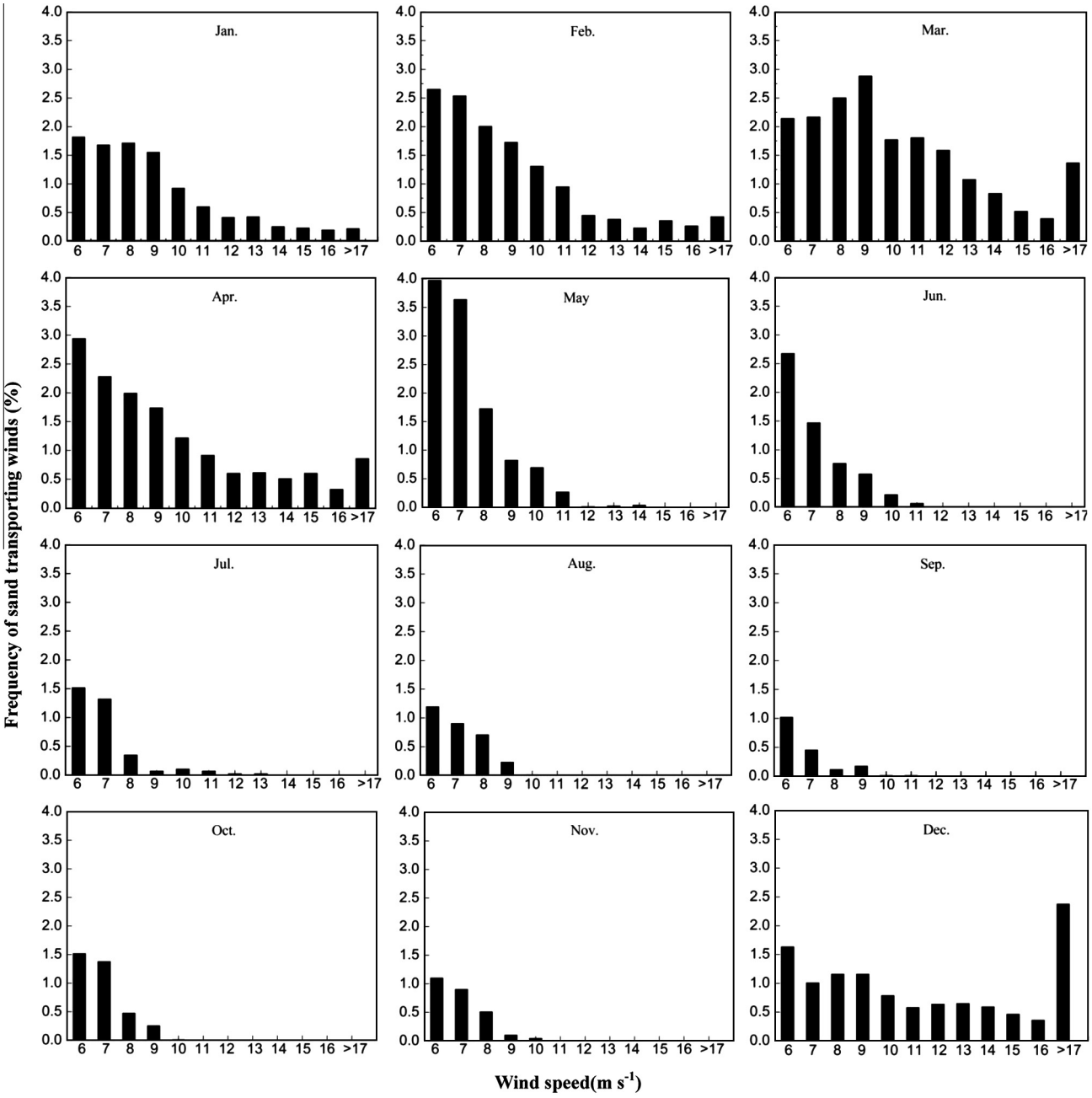

Fig. 7. Distribution of different sand-transporting wind frequencies in different months.

1983). However, these barchans are asymmetric owing to the occurrence of three prevailing wind directions, mirroring the morphology that has been observed elsewhere on Earth and other planets (Fig. 9) (Mainguet, 1984; Radebaugh et al., 2010; Bourke, 2010).

4.2. Sand-transporting events

We detected a total of 752 sand-transporting events during the study period. The monthly distribution of all sand-transporting events is illustrated in Fig. 10. The highest and lowest frequency of sand-transporting events occurred in spring and autumn, respectively. Moreover, the highest and lowest number of sand-transporting events occurred during February and September, respectively. The durations of sand-transporting events were from 10 to 1940 min. The average duration of all sand-transporting events was 110 min, whereas we observed 255 events that lasted for only 10 min. Sand-transporting events were also found to occur at certain times of a day, with the most occurring during 14:00–18:00 and the least occurring during 06:00–08:00 AM (the local time) (Fig. 11). Overall, more sand-transporting events occurred during daytime than during the evening, although nine events lasted for an entire day. These results were in agreement with the daily patterns of dust storms described by Yao et al. (2011). The sand-transporting events observed here were consistent with daily patterns of wind speed variation and were likely related to air temperatures and amounts of solar radiation.

4.3. Comparison of the wind regime with other neighboring stations

During the study period, the drift potential (DP) of the study area was higher than that of the Bayanmao Dao, Guaizihu, Ejina Qi and Minqin stations, particularly in spring and winter (Fig. 12). Our study area is located between the Yabrai Mountains

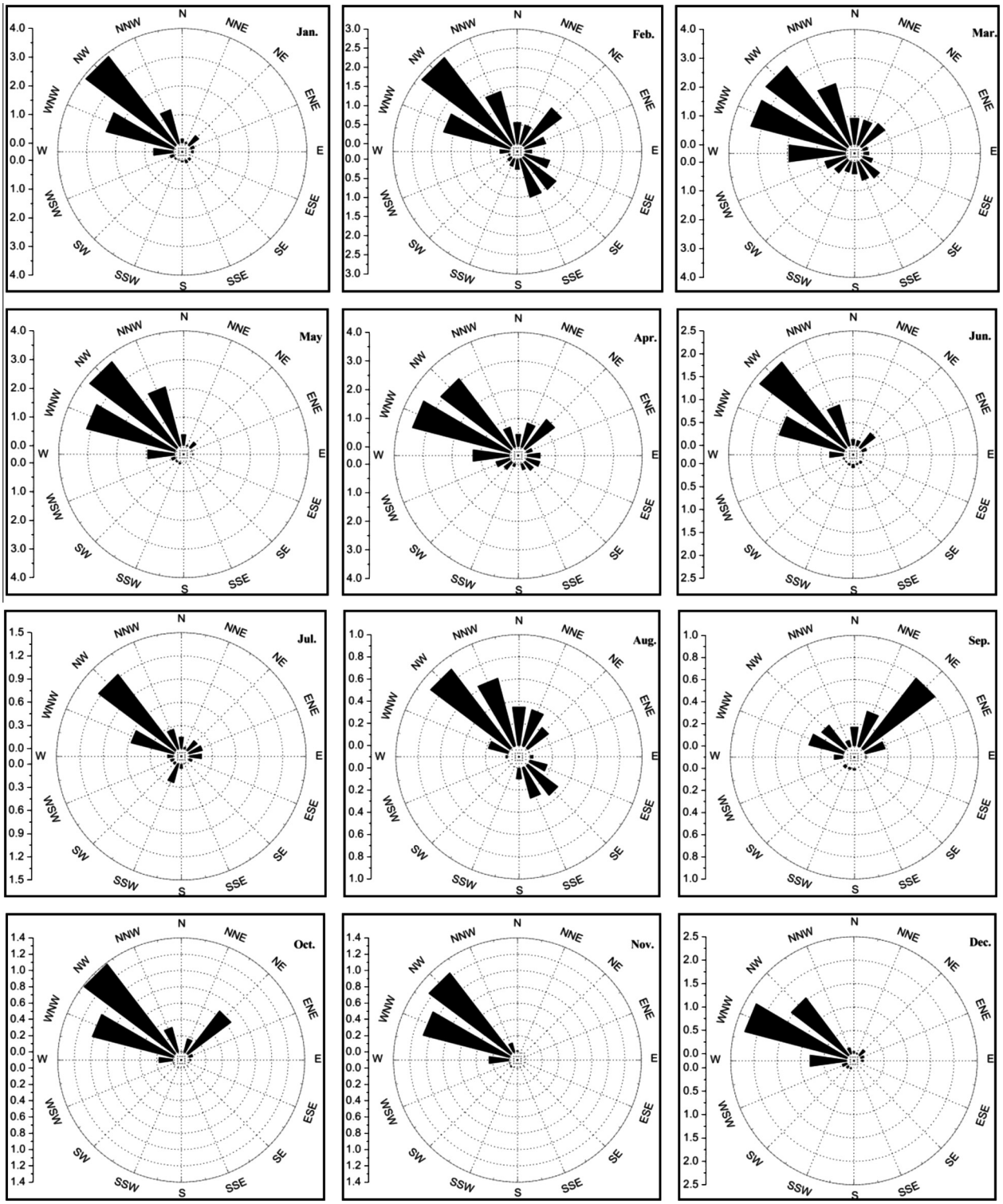

Fig. 8. Distribution of frequency (%) of sand-transporting winds in different directions in different months.

and the Allah Teng Mountains, and thus, it was likely that funneling led to increased near surface airflow and wind speeds. The resultant DP in the study area was 729.3 vector units (VU), indicating a high-energy wind regime, whereas the DPs at the Bayanmao Dao, Guaizihu, Ejina Qi and Minqin stations were 162.1, 195.6, 57.8 and 74.1 VU, respectively. In general, the DPs of the other stations have decreased since 1973 and reached a minimum in 2011, particularly at the Minqin and Bayanmao Dao stations (Fig. 13). Because these two stations are located relatively near the study area, we assumed that the DP of our study area has also decreased since 1973 and reached its minimum value in the study year. The wind direction of different months in the study area was concentrated and similar to that observed at Bayanmao Dao, although the direction in other stations varied significantly.

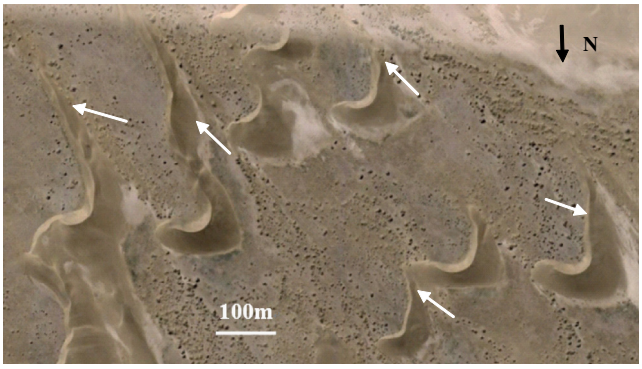

Fig. 9. Examples of asymmetric barchans dunes in the corridor (40°01′07.58″N, 103°56′48.66″E). The main wind directions that formed the barchans are oblique to the elongated right horn. Image used with permission from Google Earth. The white arrows point to the asymmetric horn.

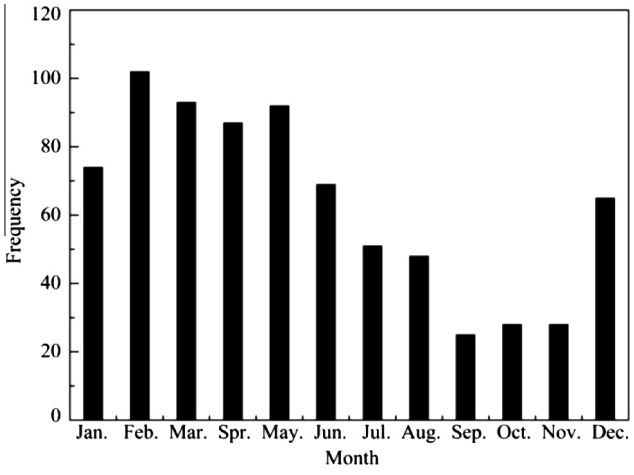

Fig. 10. Frequency of sand-transporting events in different months.

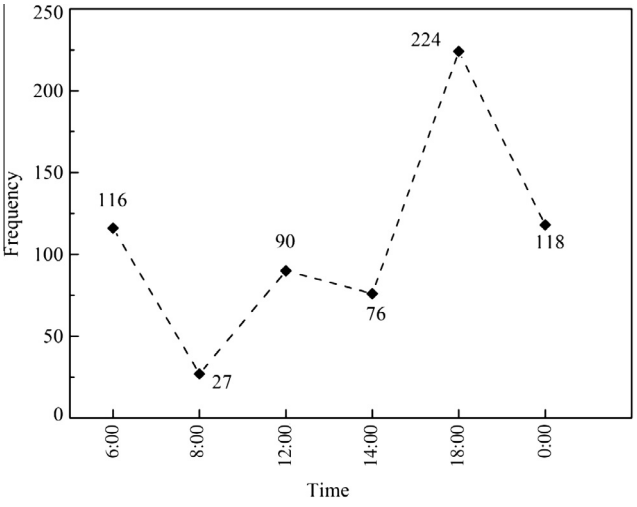

Fig. 11. Frequency of sand-transporting events during different periods. 0:00–6:00 (the local time) is the wee hours of the morning; 6:00–8:00 is the morning; 8:00–12:00 is the time between morning and noon. 12:00–14:00 is the noon; 14:00–18:00 is the afternoon; 18:00–0:00 is the night.

4.4. Sand transport flux

4.4.1. Seasonal and directional variation of sand transport flux

The resultant flux of sand transported from the BJ to the Tengger desert over the entire year was 372 tons m^{-1}, with transport direction primarily in SE (Table 3). This sand transport flux is greater than those in the Mu Us sandy land, Qubqi desert (Liu et al., 2005), and the desert of Kuwait (Al-Awadhi and Al-Awadhi, 2009). Moreover, based on the low DP during the study period (Zhang et al., 2011), the annual sand transport flux during the studied year may be the lowest in the past 40 years.

The sand transport in spring and winter represented 99.8% of the resultant sand transport flux. In particular, the greatest sand transport (161 tons m^{-1}) was in December, accounting for 43.4% of the resultant. Conversely, the lowest sand transport (0.7 tons m^{-1}) was in September and accounted for only 0.2% of the resultant. Sand transport directions varied in different months but generally fell within the range 119–152° (Table 3).

The percentages of amount of sand transported in the WNW, NW and NNW directions were 36.4%, 34.8% and 6.1%, respectively, accounting for 77.3% of the total sand transport during the study period. The greatest amount of sand transported (approximately 172 tons m^{-1} yr^{-1}) occurred in the WNW direction, whereas sand-transporting winds occurred most frequently in the NW direction in February and March. This resulted in greater amounts of sand being transported in the direction in these months with amounts of 21 and 39 tons m^{-1} (Table 4).

4.4.2. The influence of wind on sand transport flux

Sand transport is influenced by wind direction, magnitude and frequency (Liu et al., 2005; Hu et al., 2009). With the decreasing of sand-transporting wind frequency and increasing of wind speed, the amount of sand transport has increased firstly, reached the maximum at the speed of 10 m s^{-1} and then decreased. The frequency of wind speed at 6 m s^{-1} was the highest, whereas the amount of sand transported was the lowest. Therefore, the amount of sand transport is influenced by both frequency and magnitude of wind speed (Table 5). Our results demonstrate that 50.5% of total sand transport occurred owing to normal (i.e., <17 m s^{-1}) high-frequency sand-transporting winds, whereas the remaining 49.5% transport occurred owing to strong winds, particularly those in December. Therefore, the proportions of sand transported by the normal and strong winds were almost equal, despite the inherent difference in transport mechanisms, namely, the normal sand-transporting winds achieved such high sand transport flux owing to their higher frequency, whereas the strong winds achieved such flux owing to their high energy. In our study area, the relatively high frequencies of strong winds led to a large amount of sand transport. In particular, two continuous sand and dust storms were observed during the study period. The first lasted for 900 min from 18:10 (the local time) on December 27, 2010 until 02:00 AM on December 28, 2010, and the other lasted for 1940 min from 11:00 AM on December 28, 2010 to 17:10 on December 29, 2010. During the second sand-transporting event, the maximum instantaneous wind speed was 28.6 m s^{-1} and the amount of sand transported was 86 tons m^{-1}, which accounted for 23.1% of the resultant amount of sand transported throughout the study period (Table 5).

4.4.3. The sand transport flux of sand-transporting events

Fig. 14 illustrates the amount of sand transported during each transporting event in each month. The maximum amount of sand transported of transporting events was 86 tons m^{-1} in December, whereas the minimum amount was 0.06 kg m^{-1} in every month. The amounts of each sand-transporting event varied by five orders of magnitude. In spring (except May) and winter, the amount of

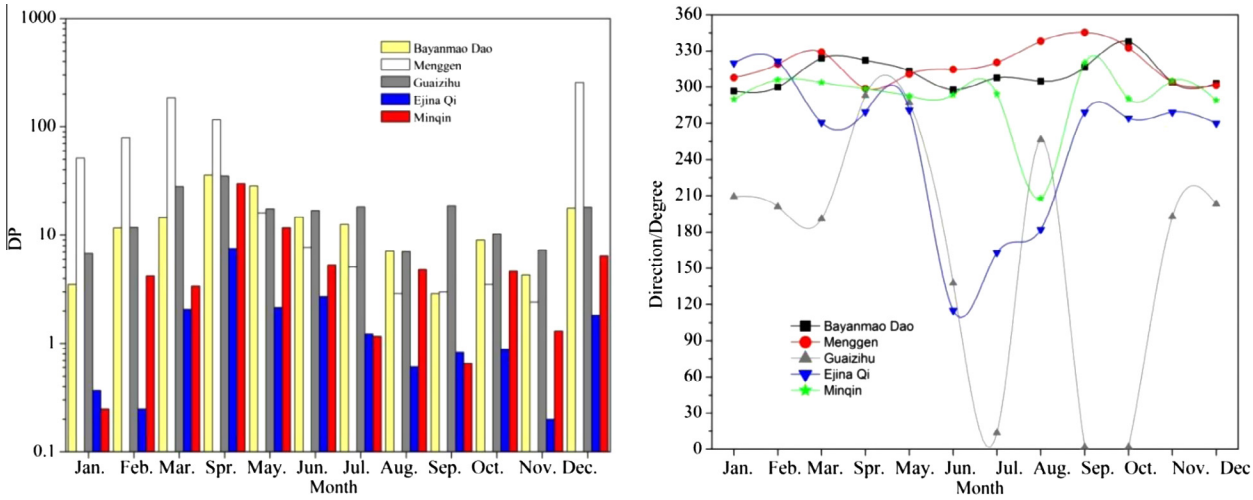

Fig. 12. Drift potential and direction of study area and neighboring stations in different months (left: drift potential, right: direction). DP is drift potential. Unit of DP is vector unit (VU).

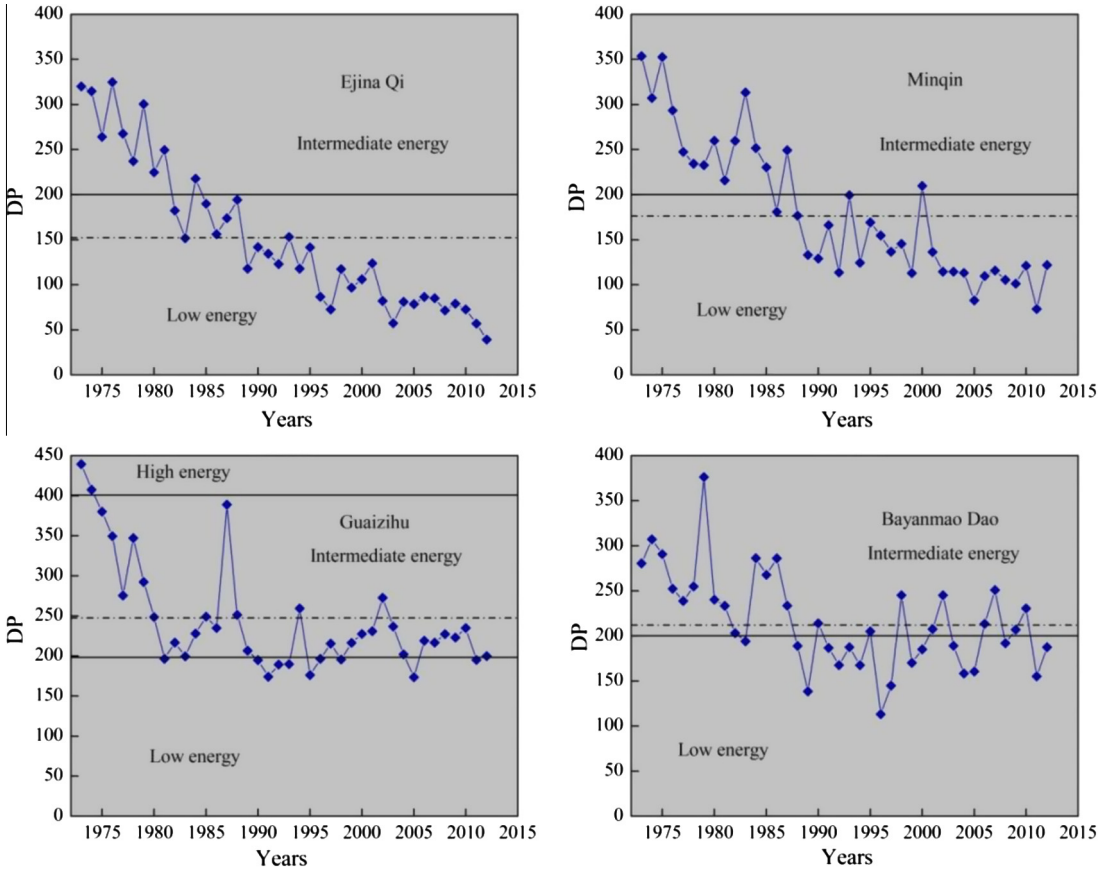

Fig. 13. Yearly variation in DP for 4 neighboring stations. DP is drift potential. Unit of DP is VU. Dash line is the average drift potential and black line is the drift potential levels. Low energy is DP < 200; intermediate energy is 200 < DP < 400; and high energy is DP ⩾ 400.

Table 3
The amounts and directions of sand transported in each month and year. Unit is tons m^{-1}.

Amounts and directions	Months												
	Jan.	Feb.	Mar.	Apr.	May	Jun.	Jul.	Aug.	Sep.	Oct.	Nov.	Dec.	Year
Amouts of sand transport	18.34	39.39	79.94	62.96	9.09	4.18	1.47	1.54	0.73	1.40	1.58	161.12	371.55
Directions of sand transport	149°	126°	119°	152°	140°	13 7°	139°	116°	128°	110°	145°	148°	130°

Table 4
The amounts of sand transported in different directions in different months. Unit is tons m^{-1}.

Directions	Jan.	Feb.	Mar.	Apr.	May	Jun.	Jul.	Aug.	Sep.	Oct.	Nov.	Dec.	Total (tons m^{-1} yr^{-1})
N	0.23	1.61	3.71	0.96	0.35	0.02	0.18	0.26	0.04	0.02	0.02	0.01	7.41
NNE	0.02	6.23	10.32	1.19	0.04	0.03	0.00	0.11	0.06	0.21	0.00	0.05	18.26
NE	0.14	2.13	18.92	2.02	0.36	0.06	0.02	0.14	0.12	0.55	0.00	0.31	24.78
ENE	0.07	1.01	2.58	0.25	0.05	0.01	0.02	0.00	0.00	0.02	0.00	0.27	4.27
E	0.05	0.45	0.92	0.74	0.07	0.00	0.01	0.00	0.00	0.01	0.00	1.49	3.74
ESE	0.00	1.24	1.16	0.95	0.00	0.00	0.00	0.02	0.00	0.00	0.00	0.00	3.37
SE	0.02	1.66	2.36	1.18	0.00	0.00	0.00	0.03	0.00	0.00	0.00	0.00	5.26
SSE	0.02	0.94	2.29	1.17	0.00	0.01	0.01	0.02	0.00	0.00	0.00	0.00	4.45
S	0.01	0.12	1.48	0.07	0.01	0.01	0.03	0.01	0.00	0.00	0.00	0.01	1.73
SSW	0.00	0.10	0.59	0.04	0.00	0.00	0.08	0.00	0.00	0.00	0.00	0.26	1.06
SW	0.03	0.07	0.75	0.08	0.00	0.00	0.01	0.00	0.00	0.00	0.01	0.92	1.88
WSW	0.28	0.19	1.48	2.81	0.08	0.02	0.02	0.00	0.00	0.00	0.01	1.03	5.92
W	2.04	1.53	6.58	10.29	0.65	0.17	0.08	0.00	0.02	0.08	0.07	8.31	29.83
WNW	11.38	12.54	23.22	35.62	3.71	1.11	0.30	0.17	0.32	0.51	0.67	82.48	172.03
NW	2.93	21.33	39.05	20.28	3.73	2.12	0.97	0.78	0.29	0.50	0.79	73.43	166.18
NNW	2.93	6.23	14.14	1.38	1.34	0.97	0.11	0.40	0.08	0.17	0.09	2.32	30.15

Table 5
The amounts of sand transported at different wind speed levels in different months. Unit is tons m^{-1}.

Wind speed (m/s)	Jan.	Feb.	Mar.	Apr.	May	Jun.	Jul.	Aug.	Sep.	Oct.	Nov.	Dec.	Total (tons m^{-1} yr^{-1})
6	0.22	0.37	0.31	0.40	0.58	0.37	0.20	0.13	0.37	0.26	0.16	0.21	3.56
7	1.01	1.38	1.25	1.25	2.00	0.78	0.69	0.51	0.25	0.76	0.51	0.61	11.01
8	2.06	2.39	3.00	0.01	1.99	1.30	0.37	0.82	0.14	0.53	0.61	1.37	14.60
9	3.28	3.85	6.09	3.64	1.65	1.18	0.15	0.45	0.33	0.50	0.21	2.47	23.80
10	2.98	4.16	5.80	3.91	2.22	0.71	0.36	0.03	0.04	0.03	0.17	2.55	22.96
11	2.85	4.52	8.61	4.33	1.25	0.33	0.35	0.00	0.00	0.00	0.00	2.80	25.04
12	2.83	2.99	10.69	4.16	0.07	0.23	0.18	0.00	0.03	0.00	0.00	4.37	25.53
13	3.93	3.48	9.67	5.72	0.22	0.00	0.21	0.00	0.00	0.00	0.00	5.88	29.11
14	3.00	2.82	9.89	6.11	0.40	0.00	0.00	0.00	0.00	0.00	0.00	7.29	29.51
15	3.47	5.44	7.90	9.00	0.00	0.00	0.00	0.00	0.00	0.00	0.00	7.12	32.91
16	3.78	4.91	7.51	6.07	0.00	0.00	0.00	0.00	0.00	0.00	0.00	6.87	29.13
17	1.90	3.14	5.49	2.17	0.00	0.00	0.00	0.00	0.00	0.00	0.00	4.58	17.27
18	2.61	1.88	7.66	7.17	0.00	0.00	0.00	0.00	0.00	0.00	0.00	6.92	26.23
19	0.79	1.19	4.69	5.76	0.00	0.00	0.00	0.00	0.00	0.00	0.00	8.91	21.33
20	0.92	2.41	7.90	3.22	0.00	0.00	0.00	0.00	0.00	0.00	0.00	10.66	25.10
21	0.00	3.20	10.81	3.68	0.00	0.00	0.00	0.00	0.00	0.00	0.00	10.25	27.94
22	0.00	0.00	1.99	6.82	0.00	0.00	0.00	0.00	0.00	0.00	0.00	13.92	22.73
23	0.00	3.60	3.72	2.14	0.00	0.00	0.00	0.00	0.00	0.00	0.00	14.69	24.14
24	0.00	0.00	4.98	0.00	0.00	0.00	0.00	0.00	0.00	0.00	0.00	23.54	28.52
25	0.00	0.00	3.76	0.00	0.00	0.00	0.00	0.00	0.00	0.00	0.00	12.45	16.21
26	0.00	0.00	6.47	0.00	0.00	0.00	0.00	0.00	0.00	0.00	0.00	9.68	16.14
27	0.00	0.00	0.00	0.00	0.00	0.00	0.00	0.00	0.00	0.00	0.00	6.18	6.18
28	0.00	0.00	0.00	0.00	0.00	0.00	0.00	0.00	0.00	0.00	0.00	4.10	4.10

sand transported by events that transported more than 100 kg m^{-1} accounted for 26.8–35.1% of the resultant amount of sand transported in each month. Conversely, in summer, such events contributed only 9.7–11.5% of resultant sand transport and more than 60% of sand-transporting events transported less than 10 kg m^{-1} of sand. Similarly, in spring (except May) and winter, the amount of sand transported by events that transported more than 1000 kg m^{-1} occurred over 10% of the resultant amount of sand transported in each month, whereas very few events transported more than 1000 kg m^{-1} of sand in summer (except June) and autumn.

4.4.4. The verification of resultant sand transport flux

To validate the results, we selected ten barchan dunes in the study area at random and measured the speeds of migration and morphological parameters. According to Bagnold (1941),

$$Q_d = C \times H \times \gamma,$$

where Q_d is the amount of sand transported through dune migration (measured in kg m^{-1} yr^{-1}), C is the speed of dune migration (m yr^{-1}) and γ is the density of dry sand (which we assume to be 2200 kg m^{-3}). The speed of dune migration has been estimated to be 7–13 m yr^{-1} during 1999–2009, and is thought to depend on the height (size) of the dunes (Gay, 1999; Andreotti et al., 2002). In the present study, the direction of dune migration was 119–133°, which corresponds to the resultant drift direction of 130° in Table 6. The morphologies of barchans changed differently, and sand transport flux through dune migration was 257–323 tons m^{-1} yr^{-1}, which is considerably less than our previous estimate of 372 tons m^{-1} yr^{-1}. In the present study, we have not considered vegetation cover, the moisture conditions of surface sediments or the geomorphologic setting. The study area is located in shifting sandy drylands, where vegetation cover is <5% (Zhu et al., 1980), particularly in spring and winter. Therefore, the influence of vegetation on sand transport could be negligible. Furthermore, the study area lies within the transition zone between arid and extremely arid conditions (Ye and Chen, 1992), where evaporation far exceeds precipitation (Liu, 2004), and moisture at the sediment surface is very limited, except during rainy or snowy days. Typically, precipitation is concentrated in summer when the amounts of sand transported are relatively low. Thus, the influence of moisture on the study area is also low. And we only focused on sand transport in both shifting sand dune and inter-dune flat areas. However, it is possible that we have overestimated sand transport in winter,

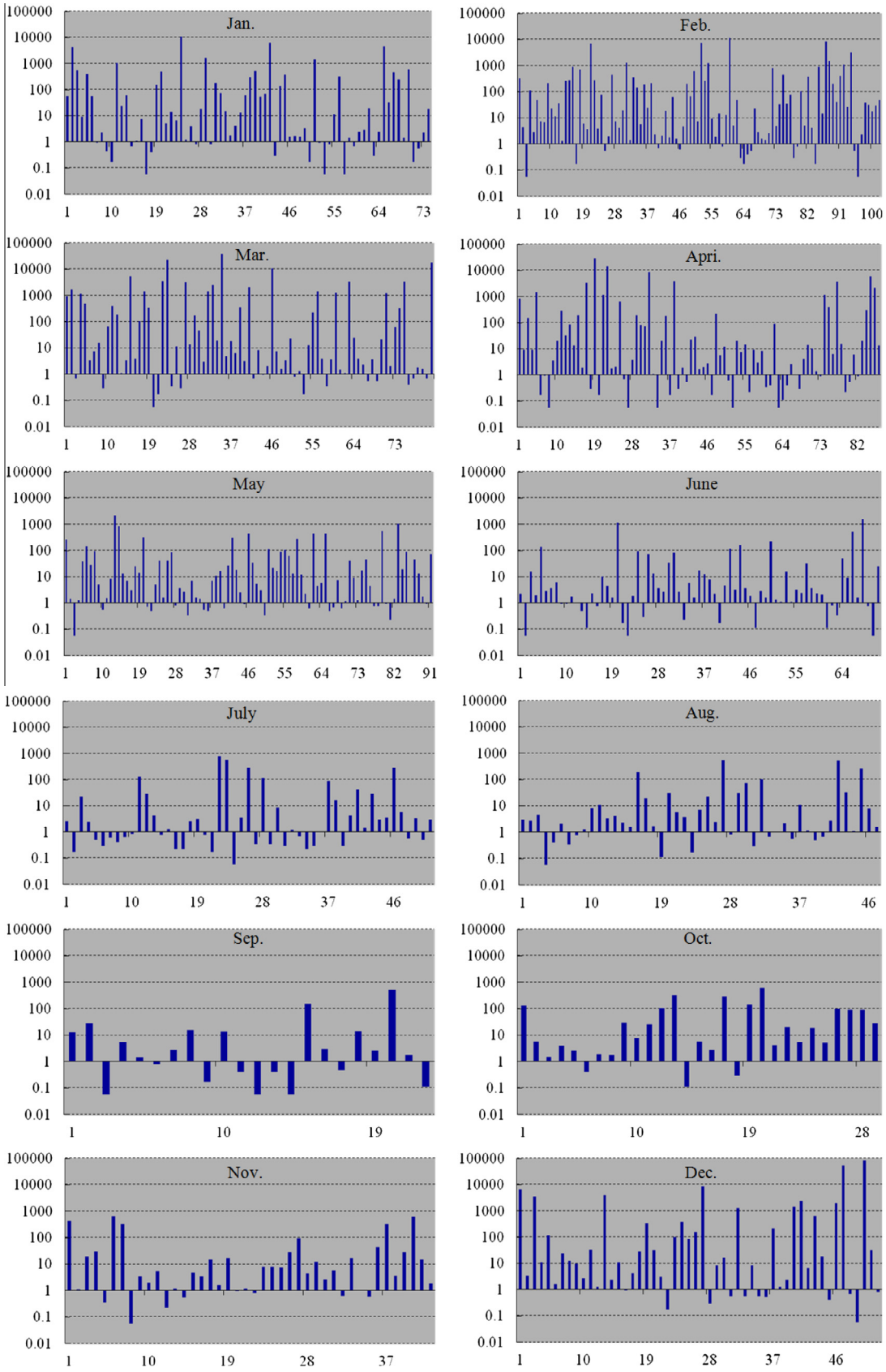

Fig. 14. The amounts of sand transported of each sand-transporting event in different months.

when snowfall, low temperatures and sand-transporting events occur simultaneously. Therefore, snowfall and low temperatures in winter may have reduced dune migration and affected sand transport. The difference of sand transport between the two methods was only approximately 10%. Our estimate value of sand transport flux of 372 tons m^{-1} yr^{-1} differed by an order of

Table 6
Dunes morphological parameters, speeds and amounts of sand transported of barchans dunes migration in 1999–2009.

No.	Latitude	Longitude	Data (year)	Width (m)	Length (m)	Left horn length (m)	Right horn length (m)	Perimeter (m)	Area (m^2)	Height (m)	Migration distance (m)	Migration speed ($m\ yr^{-1}$)	Q_d (tons $m^{-1}\ yr^{-1}$)	Directions (°)
1	40°4′50″N	103°56′26″E	1999	282	373	216	100	1167	43,376	9	132	13	257	123
			2009	294	522	320	80	1436	53,105					
2	40°4′34″N	103°56′8″E	1999	310	370	157	140	1262	61,862	14	98	10	308	126
			2009	272	339	110	115	1164	61,760					
3	40°3′33″N	103°55′34″E	1999	326	245	105	88	1074	53,771	12	110	11	290	130
			2009	280	283	128	71	982	44,035					
4	40°4′35″N	103°53′17″E	1999	366	267	100	133	1119	52,829	21	65	7	323	129
			2009	376	328	128	120	1233	60,165					
5	40°4′50″N	103°53′6″E	1999	266	190	63	124	860	30,539	15	88	9	297	126
			2009	252	221	69	83	851	31,226					
6	40°5′50″N	103°51′17″E	1999	278	220	59	112	899	33,437	20	69	7	308	128
			2009	293	258	120	112	980	36,466					
7	40°6′34″N	103°51′55″E	1999	334	318	122	130	1153	51,017	18	79	8	317	132
			2009	287	278	83	113	1099	51,323					
8	40°7′24″N	103°50′16″E	1999	318	281	101	162	1113	48,102	16	83	8	282	133
			2009	347	286	84	123	1105	52,209					
9	40°7′48″N	103°47′19″E	1999	385	306	120	135	1219	57,165	26	55	5	286	118
			2009	443	315	150	161	1390	65,628					
10	40°6′12″N	103°52′14″E	1999	397	242	86	142	1253	62,807	21	67	7	323	130
			2009	432	347	120	122	1498	85,819					

magnitude from those of Yao (2006), who suggested sand transport flux was 32 tons $m^{-1}\ yr^{-1}$ based on neighboring station (Bayan Nuru) wind speeds at a 10 m height.

4.5. The annual total amount of sand transport

The width of the corridor in our measurement field is approximately 28 km which includes shifting sand dune area (the length is 5.5 km) and inter-dune flat area (the length is 22.5 km). The amount of sand transported in the inter-dune flat area is almost 37% of bulk flux (Wiggs, 1992). The total amount of sand transported is the sum of bulk flux and inter-dune flux (Sarnthein and Walger, 1974). Therefore, the total amount of sand transported across the corridor was over 5 million tons yr^{-1}. Based on these data, the sand transported from the BJ to the Tengger desert could cover the Tengger desert by a thickness of 0.6 mm each year (based on the Tengger desert having an area of 36,700 km^2). Approximately 16,000 years the Tengger desert can be increased by 1 m because of the sands transported from the BJ desert through this corridor if the atmospheric condition was similar to the present situation all through the time.

5. Conclusions

We measured wind speeds at a 2 m height above the ground for the period from November 2010 to December 2011 in one of the corridors between the BJ and the Tengger deserts. Our results showed that sand-transporting winds accounted for 16.4% of the entire year duration and occurred mostly in spring and winter. The prevailing wind directions were NW, WNW and NNW, making up 61.9% of the total frequency of sand-transporting winds. The frequencies of winds decreased with increasing wind speed, and the frequency of strong winds made up 5.3% of the sand-transporting winds. In total, 752 sand-transporting events were detected, with the period of 14:00 to 18:00 (afternoon) containing the greatest number of sand-transporting events. The resultant drift potential for the study period was 729.3 VU, indicating a high-energy wind regime. This value was higher than those recorded at neighboring stations, illustrating an obvious effect of narrowing.

Our estimate value of sand transport flux of 372 tons $m^{-1}\ yr^{-1}$ is larger by an order of magnitude than that of Yao (2006) who suggested sand transport flux was 32 tons $m^{-1}\ yr^{-1}$. The sand transport direction was 130°. The speed of dune migration in the study area was 7–13 m yr^{-1}. The resultant amount of sand transported calculated with two methods could be calibrated and validated each other. The annual total amount of sand transport across the corridor was over 5 million tons, with 77.3% being transported by the prevailing winds, indicating a substantial sand supply from the Badain Jaran to Tengger desert. Moreover, the amount of sand transported in the spring and winter accounted for 99.8% of total sand transport. The amount of sand transported during different transporting events varied by five orders of magnitude, ranging from 0.06 kg m^{-1} to 86 tons m^{-1}. Additionally, both normal sand-transporting winds and strong winds played dominant roles in sand transport in the study area, despite the different transport mechanisms involved.

The results of sand transport in the corridor may help to elucidate the contribution of the BJ to the Tengger desert, the ecological impact of sand encroachment on adjacent oases, and the construction of sand-fixing protection systems.

Acknowledgments

We gratefully acknowledge the funding received from the Natural Science Foundation of China (Grant Nos. 41071331, 41321001 and 41201261). We also extend our sincere thanks to the two anonymous referees and the editors for their invaluable comments, and Professors ZhongPing Lai and Ming Wang, who gave generous help to improve the manuscript.

References

Al-Awadhi, J.M., Al-Awadhi, A.A., 2009. Modeling the aeolian sand transport for the desert of Kuwait: constraints by field observations. J. Arid Environ. 73, 987–995.
Anderson, R.S., Haff, P.K., 1988. Simulation of aeolian saltation. Science 241, 820–823.
Andreotti, B., Claudin, P., Douady, S., 2002. Selection of dune shapes and velocities. Eur. Phys. J. B 28, 321–339.
Bagnold, R.A., 1936. The movement of desert sand. Proc. R. Soc. Lond. A 157, 594–620.
Bagnold, R.A., 1937. The transport of sand by wind. J. Geogr. Sci. 89, 409–438.

Bagnold, R.A., 1941. The Physics of Blown Sand and Desert Dunes. Chapman and Hall, London, pp. 104–106.
Barchyn, T.E., Hugenholtz, C.H., 2012. Winter variability of aeolian sediment transport threshold on a cold-climate dune. Geomorphology 177–178, 38–50.
Bourke, M.C., 2010. Barchan dune asymmetry: observations from Mars and Earth. Icarus 205, 183–197.
Buckley, R.C., 1987. The effect of sparse vegetation on the transport of dune sand by wind. Nature 325, 426–428.
Central Meteorological Bureau of China, 1994. Climatic Atlas of the People's Republic of China. The Map Publishing House, Beijing, p. 226 (in Chinese).
Chen, J.S., Li, L., Wang, J.Y., Barryll, B.A., Sheng, X.F., Gu, W.Z., Zhao, X., Chen, L., 2004. Groundwater maintains dune landscape. Nature 432, 459–460.
Deganto, A.T., 1997. A quality control routine for hourly wind observations. J. Atmos. Ocean. Technol. 14, 308–317.
Dong, Z., 2004. Research on farmland wind–sand disaster of oasis and its contral mechanism in Ulan Buh desert. Ph.D. Thesis, Beijing Forestry University (in Chinese).
Dong, Z.B., Wang, T., Wang, X.M., 2004. Geomorphology of the megadunes in the Badain Jaran desert. Geomorphology 60, 191–203.
Dong, Z.B., Qian, G.Q., Li, B.S., Luo, W.Y., Zhang, Z.C., Xiao, S.C., Zhao, A.G., 2009. Geomorphological hierarchies for complex mega–dunes and their implications for mega–dune evolution in the Badain Jaran desert. Geomorphology 106, 180–185.
Dong, Z., Zhang, Z., Lv, P., Qian, G., 2011. An aeolian transport model for flat shifting sand fields under dynamic–limiting conditions. J. Arid Environ. 75, 865–869.
Dong, Z.B., Qian, G.Q., Lv, P., Hu, G.Y., 2013. Investigation of the sand sea with the tallest dunes on Earth: China's Badain Jaran Sand Sea. Earth-Sci. Rev. 120, 20–39.
Fryberger, S.G., Dean, G., 1979. Dune forms and wind regime. U.S. Geological Survey Professional Paper 1052–F, pp. 137–169.
Gay, S.P., 1999. Observation regarding the movement of barchan sand dunes in the Nazca to Tanaca area of southern Peru. Geomorphology 27, 279–293.
Gillette, D.A., Niemeyer, T.C., Helm, P.J., 2001. Supply-limited horizontal sand drift at an ephemerally crusted, unvegetated saline playa. J. Geophys. Res. 106, 18085–18098.
Guo, H.D., 1986. Space shuttle radar response from sand dunes and subsurface rocks of Alax Plateau. Remote Sens. Environ. 1 (1), 34–43 (in Chinese).
He, M.Z., Li, X.J., Jia, R.L., Zhang, J.G., Zheng, J.G., 2010. Environmental effects on distribution and composition of desert vegetations in Alxa Plateau: I. Environmental effects on the distribution patterns of vegetation in Alxa Plateau. J. Desert Res. 30 (1), 46–56 (in Chinese).
Hesp, P., Davidson-Arnott, R., Walker, I., Ollerhead, J., 2005. Flow dynamics over a foredune at Prince Edward Island Canada. Geomorphology 65, 71–84.
Hu, X., Liu, L.Y., Li, S.J., Xiao, B.L., Liu, M.X., 2009. Estimation of sand transportation rate for fixed and semi-fixeddunes using meteorological wind data. Pedosphere 19 (1), 129–136.
Iversen, J.D., Rasmussen, K.R., 1994. Effect of slope on saltation threshold. Sedimentology 41, 721–728.
Jackson, N.L., Nordstrom, K.F., 1998. Aeolian transport of sediment on a beach during and after rainfall, Wildwood, NJ, USA. Geomorphology 22, 151–157.
Kawamura, R., 1951. Study of sand movement by wind. The reports of the Institute of Science and Technology, vol. 5. University of Tokyo, Tokyo, Japan, pp. 95–112.
Kuriyama, Y., Mochizuki, N., Nalashima, T., 2005. Influence of vegetation on Aeolian sand transport rate from a backshore to a foreshore at Hasaki, Japan. Sedimentology 52, 1123–1132.
Lancaster, N., 1985. Winds and sand movements in the Namib sand sea. Earth Surf. Proc. Land. 10, 607–619.
Lancaster, N., 2006. Linear dunes on Titan. Science 312, 702–703.
Lee, E.H., Sohn, B.J., 2011. Recent increasing trend in dust frequency over Mongolia and Inner Mongolia regions and its association with climate and surface condition change. Atmos. Environ. 45, 4611–4616.
Lei, J.Q., Wang, X.Q., Wang, D., 2003. The formation of the blown sand disaster to the Tarim desert highway, Xinjiang, China. Arid Zone Res. 20 (1), 1–6 (in Chinese).
Lettau, H., Lettau, H.H., 1978. Experimental and micro–meteorological field studies of dune migration. IES Report 101. In: Leattau, H.H., Lettau, K. (Eds.), Exploring the World's Driest Climate. University of Wisconsin, Madison, pp. 110–147.
Leys, J.F., Eldridge, D.J., 1991. Influence of cryptogamic crust disturbance to wind erosion on sand and loam rangeland soils. Earth Surf. Proc. Land. 23 (11), 963–974.
Liu, A.X., 2004. Remote sensing monitoring of desertifieation in China and Central Asia. Ph.D. Thesis, Chinese Academy of Science (in Chinese).
Liu, L.Y., Skidmore, E., Hasi, E., Wagner, L., Tatarko, J., 2005. Dune sand transport as influenced by wind directions, speed and frequencies in the Ordos Plateau, China. Geomorphology 67, 283–297.
Mainguet, M., 1984. A classification of dunes based on aeolian dynamics and the sand budget. In: El-Baz, F. (Ed.), Deserts and Arid Lands. Martinus Nijhoff, Boston, pp. 31–58.
Owen, P.R., 1964. Saltation of uniform grains in air. J. Fluid Mech. 20, 225–242.
Qu, J.J., Chang, X.L., Dong, G.R., Wang, X.Z., Lu, J.H., Zhong, D.C., 2003. Fractal behavior of aeolian sand landform in typical mega–dune area of Badain Jaran desert. J. Desert Res. 23 (4), 361–365 (in Chinese).
Radebaugh, J., Lorenz, R., Farr, T., Paillou, P., Savage, C., Spencer, C., 2010. Linear dunes on Titan and earth: Initial remote sensing comparisons. Geomorphology 121, 122–132.
Rice, M.A., McEwan, I.K., 2001. Crust strength:a wind tunnel study of the effect of impact by saltating particles on cohesive soil surfaces. Earth Surf. Proc. Land. 26 (7), 721–733.
Sarnthein, M., Walger, E., 1974. Der äolische Sandstrom aus der W-Sahara zur Atlantikkuste. Geol. Rundsch. 63, 1065–1087.
Sherman, D.J., Li, B.L., 2012. Predicting aeolian sand transport rates: a reevaluation of models. Aeol. Res. 3, 371–378.
Sherman, D.J., Jackson, D.W.T., Namikas, S.L., Wang, J., 1998. Wind–blown sand on beaches: an evaluation of models. Geomorphology 22, 113–133.
Sherman, D.J., Li, B.L., Ellis, J.T., Farrell, E.J., Maia, L.P., Granja, H., 2013. Recalibrating aeolian sand transport models. Earth Surf. Proc. Land. 38, 169–178.
Sørensen, M., 2004. On the rate of aeolian sand transport. Geomorphology 59, 53–62.
Stout, J.E., 2004. A method for establishing the critical threshold for aeolian transport in the field. Earth Surf. Process. Land. 29, 1195–1207.
Stout, J.E., 2007. Simultaneous observations of the critical aeolian threshold of two surfaces. Geomorphology 85, 3–16.
Wang, T., 1990. Formation and evolution of Badain Jaran desert. Chin. J. Desert Res. 10 (1), 29–40 (in Chinese).
Wang, T., Chen, G.T., Qian, Z.A., Yang, G.S., Qu, J.J., Li, D.L., 2001. Situation of sand–dust storms and countermeasures in north China. J. Desert Res. 21 (4), 322–327 (in Chinese).
Wasson, R.J., Hyde, R., 1983. Factors determining desert dune type. Nature 304, 337–339.
Wiggs, G.F.S., 1992: Sand dune dynamics: field experimentation, mathematical modelling and wind tunnel testing. Unpublished PhD thesis, University of London.
Wiggs, G.F.S., Atherton, R.J., Baird, A.J., 2004. Thresholds of aeolian sand transport: establishing suitable values. Sedimentology 51, 95–108.
Wu, Z., 2010. Geomorphology of Wind–Drift Sands and their Controlled Engineering. Science Press, Beijing China, p. 42 (in Chinese).
Yan, M.C., Wang, G.Q., 2001. Formation and growth of high Megadunes in Bada in Jaran desert. Acta Geogr. Sin. 56 (1), 83–91 (in Chinese).
Yang, Y., 1978. Arc-shaped tectonic belt of Alxa. Acta Geol. Sin. 1, 25–32 (in Chinese).
Yang, X.P., 2000. Landscape evolution and precipitation changes in the Badain Jaran desert during the last 30000 years. Chin. Sci. Bull. 45 (11), 1042–1047 (in Chinese).
Yao, Z.Y., 2006. Aeolian sand movement and sandy desertification in the Alxa Plateau. Ph.D. Thesis, Chinese Academy of Science (in Chinese).
Yao, Z.Y., Wang, T., Han, Z.W., Zhang, W.M., Zhao, A.G., 2007. Migration of sand dunes on the northern Alxa Plateau, Inner Mongolia. Chin. J. Arid Environ. 70, 80–93.
Yao, Z.Y., Wang, T., Yang, J.P., Zhu, K.W., Zhou, L., 2008. Analysis on frequently occurrence of dust storm in the Alxa Plateau. J. Arid Land Resour. Environ. 22 (9), 54–61 (in Chinese).
Yao, Z.Y., Xiao, J.H., Li, C.X., Zhu, K.W., 2011. Regional characteristics of dust storms observed in the Alxa Plateau of China from 1961 to 2005. Environ. Earth Sci. 64, 255–267.
Ye, D.Z., Chen, P.Q., 1992. The Pre-study of Global Change in China. Meteorol. Press, Beijing, China, pp. 40–42 (in Chinese).
Zhang, H.C., Ma, Y.Z., Li, J.J., Pachur, H.J., Wunnemann, B., 1999. The Holocene Palaeoclimatic change in southern vicinity of Tengger desert. Chin. Sci. Bull. 44 (6), 550–555.
Zhang, H.C., Ma, Y.Z., Peng, J.L., Li, J.J., Cao, J.X., Qi, Y., Chen, G.J., Fang, H.B., Mu, D.F., Pachur, H.J., Wunnemann, B., Feng, Z.D., 2002. Palaeolake and palaeoenvironment between 42 and 18 kaBP in Tengger desert, NW China. Chin. Sci. Bull. 47 (23), 1946–1956.
Zhang, Z.C., Dong, Z.B., Zhao, A.G., Qian, G.Q., 2011. Relationship between sand transport and sand drift potential. J. Desert Res. 31 (4), 824–827 (in Chinese).
Zhu, Z., Wu, Z., Liu, S., Di, X., 1980. An Outline of Chinese Deserts. Science Press, Beijing (in Chinese).
Zhu, J.F., Wang, N.A., Chen, H.B., Dong, C.Y., Zhang, H.A., 2010. Study on the boundary and the area of Badain Jaran Desert based on remote sensing imagery. Prog. Geogr. 29 (9), 1087–1094 (in Chinese).
Zimbelman, J.R., 2010. Transverse aeolian ridges on Mars: first results from HiRISE images. Geomorphology 121, 22–29.
Zingg, A.W., 1953. Wind tunnel studies of the movement of sedimentary material. In: Proceedings, fifth Hydraulics Conference, Studies in Engineering, vol. 34, pp. 111–135.
Zou, X.Y., Wang, Z.L., Hao, Q.Z., Zhang, C.L., Liu, Y.Z., Dong, G.R., 2001. The distribution of velocity and energy of saltating sand grains in a wind tunnel. Geomorphology 36, 155–165.